



Published in final edited form as:

*Cancer Res.* 2012 July 15; 72(14): 3652–3663. doi:10.1158/0008-5472.CAN-12-0128.

## Temporary disruption of the blood-brain barrier by use of ultrasound and microbubbles: safety and efficacy evaluation in rhesus macaques

Nathan McDannold<sup>1</sup>, Costas D. Arvanitis<sup>1</sup>, Natalia Vykhodtseva<sup>1</sup>, and Margaret S. Livingstone<sup>2</sup>

<sup>1</sup>Department of Radiology, Brigham & Women's Hospital, Harvard Medical School, Boston, MA

<sup>2</sup>Department of Neurobiology, Harvard Medical School, Boston, MA

### Abstract

The blood-brain barrier (BBB) prevents entry of most drugs into the brain and is a major hurdle to the use of drugs for brain tumors and other central nervous system disorders. Work in small animals has shown that ultrasound combined with an intravenously circulating microbubble agent can temporarily permeabilize the BBB. Here, we evaluated whether this targeted drug delivery method can be applied safely, reliably, and in a controlled manner on rhesus macaques using a focused ultrasound system. We identified a clear safety window during which BBB disruption could be produced without evident tissue damage, and the acoustic pressure amplitude where the probability for BBB disruption was 50% was found to be half of the value that would produce tissue damage. Acoustic emission measurements appeared promising for predicting BBB disruption and damage. In addition, we performed repeated BBB disruption to central visual field targets over several weeks in animals trained to perform complex visual acuity tasks. All animals recovered from each session without behavioral deficits, visual deficits, or loss in visual acuity. Together, our findings demonstrate that BBB disruption can be reliably and repeatedly produced without evident histological or functional damage in a clinically-relevant animal model using a clinical device. These results therefore support clinical testing of this noninvasive targeted drug delivery method.

### Keywords

Brain; Novel drug delivery systems; ultrasound; blood-brain barrier; MRI

### Introduction

Many systemically-administered therapeutic agents are not effective in the central nervous system (CNS) because they are blocked by the blood-brain barrier (BBB). This barrier restricts the passage of substances except for small, hydrophobic molecules, preventing most small-molecule drugs and essentially all large-molecule drugs from reaching the brain interstitial space (1,2). It is the primary hurdle to the development and use of drugs in the CNS. Most methods that have been tested to circumvent the BBB are invasive, non-targeted, or require the development of new drug carriers that utilize endogenous transport mechanisms (3,4).

**Corresponding Author:** Nathan McDannold, 221 Longwood Avenue, Boston, MA 02115, 617 278-0605, njm@bwh.harvard.edu.

**Conflict of interest:** The lead author holds two patents on the ultrasound technique evaluated in this work. The other authors have no conflicts of interest to report.

Because of the BBB, chemotherapy has not generally been a very effective option for malignant brain tumors. While the vessels in most brain tumors do not have a fully intact BBB and can be permeable, infiltrating cancer cells and small metastatic seeds may be protected by the BBB in the surrounding intact tissue (5). Furthermore, it is known that tumor vasculature permeability is heterogeneous and that there are additional barriers to drug delivery, such as increased interstitial pressures (6). For example, work in mice suggests that the blood-tumor barrier (BTB) is only partially compromised in breast cancer metastases, and that toxic concentrations of chemotherapy agents are only achieved in a small subset of highly permeable metastases (7).

Ultrasound combined with circulating microbubbles can induce temporary BBB disruption (8,9). Acoustic waves can be noninvasively focused deeply into tissue to target the disruption to discrete regions. The mechanical interaction between the ultrasound, the microbubbles, and the vasculature transiently disassembles tight junctional complexes (10,11) and induces active transport (12), allowing agents to be delivered to the brain parenchyma. Studies in small animals have shown that this method is repeatable, is possible over a wide range of ultrasound parameters (13–16), and is capable of increasing the permeability of the BTB (17). The method can enhance delivery of therapeutics to the brain (18–20) and has been shown to improve outcomes in brain tumor and Alzheimer's disease animal models (21,22). Most of these small-animal studies found that barrier function is restored after a few hours (8–10).

This technique has the potential for use with chemotherapy in brain tumors, through enhanced drug delivery to the tumor via BTB permeabilization and to infiltrating cells through disrupting the BBB of the surrounding brain. It is noninvasive, and thus can be readily repeated to match chemotherapy schedules, and it targets the drug to only desired regions. This approach may be beneficial even in infiltrating tumors such as glioma, as studies have shown that most recurrence occurs within a few centimeters of the original tumor (23–25).

Before clinical translation, devices that are compatible with human use and feasibility studies in relevant large animal models are needed. Ultrasound systems designed for thermal ablation (without injected microbubbles) have been developed that compensate for the human skull and can focus high-intensity ultrasound accurately and noninvasively into the brain (26,27). These systems operate inside an MRI under real-time guidance and are currently being tested in clinical trials (28,29). These systems have 500–1000 array elements, and by varying the phase of the different elements they can compensate for the distortion of the ultrasound beam caused by the irregularly-shaped human skull (30) and can steer the beam away from the geometric focus of the array. Volumes are treated by steering the beam to multiple overlapping targets.

These ablation systems can be used for BBB disruption. Since the ultrasound intensity required for BBB disruption is several orders of magnitude lower than that needed for thermal ablation, skull heating is not a risk for this technique. Moreover both the targetable extent of the brain and the sonication rate can be substantially increased without risk of excessive skull heating. However, the use of microbubbles introduces different risks. When microbubbles are sonicated at high intensities, they grow in size and ultimately collapse violently, a phenomenon known as inertial cavitation. Sonication with microbubbles will cause vascular damage when exposure levels exceed inertial cavitation threshold. It is unknown whether the presence of microbubbles would increase the likelihood of damage along the beam path. Regions with high microbubble concentrations, such as large blood vessels and highly vascularized structures may be at particular risk. Regions near the skull, where reflections may increase acoustic intensity, may also be at risk. Such beam path

effects can only be assessed in a large animal model. In small animals the brain is not large enough to determine whether sonications can be targeted to deep brain structures without causing damage along the ultrasound beam path. The large focal area produced at the low ultrasound frequencies used in clinical systems make this particularly challenging. Furthermore, small animal models permit only limited evaluation of potential functional deficits induced by the BBB disruption. While feasibility tests of BBB disruption have been reported for non-human primates, to date they have not attained reproducible, safe, and predictable BBB opening (31).

Our goal was to evaluate BBB disruption induced by focused ultrasound in conjunction with a microbubble-based ultrasound contrast agent (USCA) in non-human primates using a clinical transcranial MRI-guided focused ultrasound (TcMRgFUS) system. We aimed to identify safe exposure levels for BBB disruption, to test MRI and acoustic methods for monitoring the efficacy and safety of the procedure, and to evaluate histological, behavioral and cognitive effects of repeated sonication.

## Materials and Methods

### Animals

All experiments were done in accordance with procedures approved by the Harvard Medical School Institutional Animal Care and Use Committee. Tests were performed in seven adult rhesus macaques (six male, one female, weight: 5–12 kg). Each animal was anesthetized with ketamine (15 mg/kg/h i.m.) and xylazine (0.5 mg/kg/h i.m.) or with 4 mg/kg/hr ketamine and Dexmedetomidine (0.01–0.02 mg/kg/h) and intubated. The head was shaved, and a catheter was placed in a leg vein. During the procedure the heart rate, blood oxygenation levels, and rectal temperature were monitored. Body temperature was maintained with a heated water blanket.

### Device

The device tested was the ExAblate 4000 low-frequency TcMRgFUS system (InSightec). It consists of a 30 cm diameter hemispherical 1024-element phased array transducer operating at 220 kHz coupled with a 1024-channel driving system, a treatment planning workstation, and a water cooling/circulation/degassing system. The driving system allows for individual control of the phase and amplitude for each phased array element in order to steer the focal point to different targets. The focal half-intensity width and length produced by the transducer in water were provided by the manufacturer and were 3.0 and 5.8 mm, respectively. Details on the calibration procedure used to estimate the in vivo pressure amplitudes are provided in the Supplemental Methods. The system was integrated with a clinical 3T MRI unit (GE Healthcare). Imaging was performed with a 14 cm diameter receive-only surface coil (constructed in-house). For clinical use, the hemisphere transducer is mounted on its side and coupled to a patient's head via a water-tight membrane (28); here the transducer was rotated 90° so that it could be simply filled with water like a bowl. The animal was placed supine on the table with its head tilted backwards so that the top of the head was submerged (Supplementary Fig. S1A).

Two 4.0×0.7 cm passive cavitation detectors (center frequency: 610±20 kHz) were constructed and mounted in the water on each side of the head to monitor the acoustic emission produced during sonication. The signals from these detectors were amplified, filtered, and recorded to a computer using a high-speed digitizing card (PXI-5124, National Instruments). The time signal, frequency spectra, and magnitude of the emission at different harmonics were displayed in real-time during each sonication using software developed in-house in Matlab and stored for later analysis.

## Sonications

Sonications were applied transcranially under MRI guidance (see Supplementary Methods for parameters). In monkeys 1–3 (four sessions), burst sonications were delivered to individual points in the brain (35 targets overall). In the subsequent 26 sessions (monkeys 4–7), nine locations in a 3×3 grid in a single plane were targeted during each sonication (Supplementary Fig. S1B–C). During these volumetric sonications, 10 ms bursts were applied in sequence to the nine locations. The focal point was advanced to the next location every 100–400 ms, yielding an effective pulse repetition frequency at each location of 1.1–0.28 Hz. Spacing between the targets in these volumetric sonications was 2 mm, yielding a roughly cubic region of BBB disruption with dimensions of ~1 cm<sup>3</sup>.

Overall, 185 locations or volumes were sonicated in the seven monkeys. In monkeys 1–4, a range of acoustic power levels, microbubble injection/infusion parameters and brain targets were evaluated. Targets included the thalamus, putamen, cingulate cortex, visual cortex, hippocampus, and white matter structures. Sonications centered on the lateral geniculate nucleus (LGN) included the hippocampus and part of the optic tract. The third animal was tested twice over two weeks, and the fourth was tested 13 times over 26 weeks.

In the trials that targeted single locations per sonication and in 45 volumetric sonications, the microbubble USCA (Definity, Lantheus Medical Imaging) was injected as a bolus at the start of each sonication (dose: 10 µl/kg). These sonications consisted of 10 ms bursts applied at 1 Hz for 70s. Subsequent tests at 82 locations with volumetric sonication used an infusion pump (Spectra Solaris EP, Medrad) to deliver microbubbles throughout the exposures. Most (67/82) sonications with infusion used a 20 µl/kg microbubble dose and a 150 s total sonication duration; see Supplemental Methods for more details on the infusion protocol.

## Functional testing

Monkeys 5–7 received five treatments each over 5–9 weeks with bilateral targets in the hippocampus/LGN. As the resulting MRI signal enhancement at this target was relatively weak after Gd-DPTA administration, additional bilateral targets in the primary visual cortex were sonicated in sessions 3–5 in monkey 5 and in all sessions in monkeys 6–7. The exposure level in these animals was initially determined based on acoustic emission measurements obtained with the passive cavitation detectors. If initial sonications did not result in an increase in harmonic emission, which was found previously to correlate with BBB disruption (32), sonication was repeated at increased power until an increase was observed. If wideband acoustic emission, a signature for the collapse of the microbubbles that occurs at higher energy (“inertial cavitation”) (33) was observed, the power was reduced in later sessions. Additional sonications were also tested in monkeys 5–7 in the cingulate cortex and amygdala as part of the study evaluating BBB disruption and damage thresholds.

Monkeys 5–7 underwent behavioral testing before and after the sonications to evaluate their visual acuity and higher-order cognitive abilities using an automatic touchscreen apparatus for training monkeys to perform visual discrimination tasks (34). For several hours each day, in a section of their home cages, the monkeys were given choices between two simultaneously presented symbols; they chose one by touching it, and were given a fluid reward based on the correct choice. This testing should be sensitive to any sonication-induced functional deficits in motor or visual function, memory and learning. To test visual acuity, the symbols displayed were varied in size. At the smallest size tested the monkeys would need to use their central visual fields to discriminate the symbols, so any damage to central vision would be apparent as increased errors for the smaller symbols.

## Histology

Monkeys 1–4 were sacrificed for histological examination at 24h, 2 weeks, 48h, and at ~2h after the last sonication session, respectively. The animals were anesthetized with ketamine (15mg/kg i.m.) and then euthanized with an overdose of pentothal (100mg/kg). They were then perfused transcardially with 1 L 0.9% NaCl, followed by 2 L 10% buffered formalin phosphate. The brains were removed and placed in either sucrose for frozen sectioning (monkeys 1–3) or in 10% buffered formalin phosphate for paraffin sectioning (monkey 4). Frozen sections (50  $\mu$ m) were stained with Nissl; paraffin sections (5  $\mu$ m) were stained with Haematoxylin and Eosin (H&E). Additional sections from monkey 4 were also stained with Nissl (for neurons), Luxol Fast Blue (H&E-LFB; for myelin), Bielschowsky's silver stain (for axons), and Prussian blue (for hemosiderin). Several sections were also stained with TUNEL to detect DNA fragmentation suggesting apoptosis. Monkey 4 was injected after the sonications in the last session with trypan blue, a dye used to visualize the BBB disruption after euthanasia (35). 0.08g trypan blue powder (MP Biomedical) was dissolved in 2.5 ml of 0.45% NaCl and heated until boiling. This solution was then passed through a filter (MILX GV .22UM PVDF, Millipore) and slowly injected intravenously at a dose of 0.1 g trypan blue per kg of body weight (35).

## Data analysis

Post-sonication MRI was examined to determine whether contrast enhancement was evident in the T1-weighted MRI at each targeted location or volume. No scoring metric was necessary, as this enhancement (or lack of it) was obvious. We also examined the T2\*-weighted imaging for hypointense areas produced by petechiae that occur in the case of inertial cavitation (36). To aid in distinguishing between damaged spots and anatomy that is hypointense in T2\*-weighted imaging, rigid registration was performed in monkeys 4–7 between the pre- and post-ultrasound T2\*-weighted images using 3D-Slicer (37,38). By alternating between datasets, the presence or lack of sonication-induced damage could be determined. However even with this aid, changes apparent after some sonications were subtle; those cases were categorized as “suspicious”. The enhancement and T2\*-weighted imaging analysis was used to estimate the threshold for BBB disruption and severe petechiae as a function of acoustic power. These thresholds, along with error estimates, were determined by fitting the data using logistic regression.

## Results

### Summary findings

Non-invasive transcranial sonications were applied over a range of acoustic pressure amplitudes to evaluate the thresholds for BBB disruption and tissue damage (Fig. 1A). Initial tests targeted individual locations during each sonication (35 sonicated spots in monkeys 1–3). In subsequent tests, ultrasound bursts were delivered sequentially to nine locations in a 3 $\times$ 3 grid with 2 mm spacing during each sonication (Supplementary Fig. S1, B–C) to produce volumetric BBB disruption (150 sonicated volumes in monkeys 4–7). We assessed BBB disruption by comparing T1-weighted images before and after administration of an MRI contrast agent (Gd-DPTA); only if the BBB is disrupted does this agent diffuse into the brain and produce signal enhancement. Tissue damage was assessed by comparing pre- and post treatment T2\*-weighted images. Based on prior work (36) and histological examination of these animals (see below), small hypointense regions that appear in this imaging usually correspond to extravasated erythrocytes resulting from capillary damage.

Local MRI signal enhancement after Gd-DPTA injection, indicative of successful BBB disruption, was observed in 163 of the 185 targeted locations or volumes. Small dark spots were seen in 28 of these locations in the T2\*-weighted images, 11 of which were barely

detectable and were classified as “suspicious”. The pressure amplitude where the probability for BBB disruption was 50% was 149 kPa (95% CI: 125–163 kPa); the pressure amplitude where the probability of observing tissue damage was 50% and was 300 kPa (CI: 278–341 kPa). This latter threshold was conservative and included cases where the T2\*-weighted imaging was suspicious; when only locations with definitive changes in T2\*-weighted imaging were considered, the 50% threshold increased to 358 kPa (CI: 317–451 kPa). The lowest pressure amplitudes that produced evident changes in T2\*-weighted imaging were for sonications in the thalamus (193 kPa) and visual cortex (187 kPa).

The acoustic emissions produced during sonication were monitored with two ultrasound receivers mounted on either side of the monkey’s head (Fig. 1B–D). Sonications that produced a marked increase in emission at the second and third harmonics of the TcMRgFUS device resulted in signal enhancement after Gd-DPTA administration; those that also produced wideband emission resulted in hypointense spots in T2\*-weighted imaging. Sonications without microbubbles and sonications with microbubbles but where MRI contrast enhancement was not observed (including in white matter – see below) showed only a small or no increase in harmonic emission, and no wideband emission.

### MRI findings

When single points were targeted during each sonication, the resulting BBB disruption appeared as discrete enhancing spots (dimensions: 3–6 mm, length: 5–10 mm) in T1-weighted imaging after Gd-DPTA injection (Fig. 2). No BBB disruption or other MRI-evident effects were observed away from the target areas, in the ultrasound beam path, or at the skull base, except for leakage of contrast agent that was sometimes evident in sulci or ventricles when they were included in the targeted area. Even at the highest exposure levels evaluated (444–700 kPa, tested in the first animal) where extensive petechiae and severe vascular damage was observed in histology, the effects were constrained to the focal region, and no effects were found in MRI or histology outside of the targeted region. MRI signal enhancement was not detected after Gd-DPTA injection after sonication in white matter targets (N=9).

Similar results were found with volumetric sonication. When volumes were targeted in gray matter structures such as the thalamus or putamen, contiguous volumes of signal enhancement with dimensions of ~1 cm<sup>3</sup> were observed after Gd-DPTA injection (Fig. 3A–C). However, this enhancement was not observed in white matter when it was included in the sonication volume (Fig. 3D–G). As was the case with single-location sonications, no effects were observed outside of the target volumes, even when the target was deep and close to the skull base (such as the putamen target in Fig. 3A–C) or in superficial targets, such as the visual cortex. Signal enhancement from a larger, albumin-bound contrast agent (gadofosveset trisodium) was observed, but at a substantially lower level than with Gd-DTPA (Fig. 4A–B). When the sonications overlapped sulci, the resulting enhancement was higher than in the parenchyma (Fig. 4C). Disruption was achieved with both bolus injections and continuous infusions of microbubbles.

To investigate further whether BBB disruption did occur in white matter but below the detection threshold of MRI, trypan blue was administered after the sonications in the last session in monkey 4. Three volumes were targeted centered on the boundary between the cingulate cortex and white matter lateral to it. Again, Gd-DPTA extravasation was only evident in the cortical gray matter component of the sonicated volume (Fig. 4D). However, in post-mortem examination of the brain, the targeted white matter was found to be stained lightly blue (Fig. 4E), demonstrating that BBB disruption had occurred. Gray matter was found to be deeply blue-stained in comparison.

## Histology

Monkeys 1–4 were euthanized to evaluate histological effects after sonication at different exposure levels; monkeys 1–3 to evaluate acute changes (particularly those associated with T2\* evidence of damage), and monkey 4 to evaluate both short- and long-term effects and to assess the impact of repeated BBB disruption. Sonicated regions with normal-appearing T2\*-weighted imaging showed no significant changes in histological examination, even after repeated sonication over several months. Representative examples of such cases in the cingulate and visual cortices are shown in Fig. 5.

In the cingulate targets (Fig. 5A–F), the sonicated cortical areas appeared normal overall after BBB disruption (Fig. 5A). Adjacent white matter also appeared unaffected, with normal-appearing fibers (Fig. 5B) and no evidence of demyelination (Fig. 5C). The only observed changes were a very small number of damaged capillaries, which was evidenced by tiny clusters of extravasated erythrocytes (Fig. 5D) that were presumably produced during sonication ~2h earlier. Isolated deposits of hemosiderin were also found (Fig. 5E), most likely remnants of these petechiae from sonications months earlier. Prussian blue staining confirmed that these deposits contained iron. A few dark, presumably ischemic neurons were observed in a small region in the cingulate cortex (Fig. 5F). TUNEL staining was performed in a section adjacent to this region and in several other locations. No apoptotic bodies were found.

In the visual cortex (Fig. 5G–I), the sonicated region also appeared unaffected after BBB disruption, with normal appearing cortical tissue and subcortical white matter, and no abnormalities found in or around the sulci (Fig. 5G–H). No erythrocyte extravasation or hemosiderin deposits were found in this location. Neurons appeared healthy in Nissl (Fig. 5I). The brain surface also appeared generally normal (Fig. 5J), except for some hemosiderin deposits in the meninges or adjacent tissue (Fig. 5J, inset). Since the ultrasound beam passed through the entire outer brain surface, we could not identify which sonication was responsible for these effects. Additional examples showing histological findings after BBB disruption in the LGN/hippocampus are shown in Supplemental Fig. S2.

When hypointense spots in T2\*-weighted imaging were observed, more extensive petechiae were found in histology obtained shortly after sonication. However, damage to the surrounding brain parenchyma was minimal and the nearby neurons appeared mostly unaffected. At the highest exposure levels tested (444–700 kPa, monkey 1), more severe vascular and parenchymal damage was observed. In monkey 3, hemorrhagic tissue was observed in the lateral ventricle after two bilateral sonications (315 and 223 kPa) in the thalamus. Hypointense spots were evident in the sulcus in the visual cortex in monkey 4 after one session; six months later, a few hemosiderin-filled macrophages were observed in the meninges along with parenchymal damage in the adjacent cortex. The most severe dark spots, produced in sonications in the thalamus, persisted for several months; parenchymal damage, macrophage accumulation, and clusters of hemosiderin deposits were observed in histology in these cases (Supplementary Fig. S3).

T2\*-weighted imaging was more sensitive to damage than T2-weighted imaging, as small changes that were evident in T2\*-weighted imaging were not found in T2-weighted imaging. However, two locations in monkey 3 had significant erythrocyte extravasations that were not detected in MRI. Note that we did not obtain pre-treatment images in that animal, which made it difficult to distinguish damage from other tissue structures (sulci, etc.) that were also hypointense in T2\*-weighted imaging. In subsequent sessions, comparing pre- and post-sonication T2\*-weighted imaging enabled us to detect even small changes that were not evident without the context provided by pre-sonication images.

## Functional tests

Monkeys 1–4 all recovered with no apparent behavioral deficits induced by procedures. Monkeys 1–2 had one BBB disruption session each, monkey 3 had three sessions, and monkey 4 had 13 sessions. The animals appeared normal the day following each session, eating and drinking, reaching for food items held in front of them, and displaying normal aggressive behavior to caretakers. We therefore undertook more extensive behavioral testing that would be more sensitive to neuronal damage. Monkeys 5–7 were trained to use touchscreens in their home cages to choose between pairs of stimuli to select a reward amount (Fig. 6). They chose between pairs of symbols and received a fluid reward corresponding to the chosen symbol. Numerals 0–9 corresponded to 0–9 drops and the letters X-Y-W-C-H-U-T-F-K-L-N-R-M-E-A-J represented 10–25 drops. New symbols were introduced in order, and over a period of several months all monkeys learned to accurately distinguish between 26 symbols in that they almost always chose the larger of the two choices. Accurate performance of the task thus requires motor skill, the ability to remember all 26 symbols, and the ability to see and recognize the symbols. Furthermore, we tested these monkeys with symbols varying in height from 2.2 mm to 4.5 cm. Thus we could also evaluate the monkeys' acuity. We then repeatedly targeted BBB disruption bilaterally to the lateral geniculate nucleus (LGN) and in the foveal confluence of primary visual cortex and secondary visual areas (V1, V2, V3, V4) over several weeks. If damage occurred to the LGN or central visual cortex, visual acuity should be reduced, which would be apparent as a loss of ability to discriminate the smallest symbols. Results from functional testing are shown in Fig. 6. After five sessions of volumetric BBB disruption centered on these targets, no changes were observed in the performance of the visual task, and visual acuity was unaffected. Here, the acoustic emission signal was used to guide the exposure level. In 72 out of 75 targeted volumes in these animals, no abnormalities were evident in T2\*-weighted imaging; in two of the targeted volumes we observed tiny hypointense spots in the lunate sulcus; one other target near the LGN showed a faint hypointense spot that was categorized as suspicious.

## Discussion

This work demonstrates the feasibility of reliably and repeatedly inducing focal BBB disruption without significant vascular or brain tissue damage in a clinically-relevant animal model using a TcMRgFUS system designed for human use. The disruption was possible at both deep and superficial targets, and it was always contained within the sonicated volume. Other than occasional appearance of MRI contrast in the nearby sulci, no effects were observed in the acoustic beam path, and there were no signs of internal reflections or standing waves within the intact skull that led to unexpected results. Furthermore, the animals recovered without evident behavioral effects and no changes were found in visual acuity after repeated BBB disruption at targets in the visual pathway, suggesting that the procedure did not cause functional damage.

We anticipate that the first clinical tests of this technique will be for brain tumors, where current treatment options are limited. The level of histological and functional examination employed here, which demonstrated that no significant structural or functional changes were induced by the sonications, was sufficient in our view to support clinical translation for such patients. However, we expect that the technology can have application to a broader spectrum of brain diseases and disorders, including those that are not life-threatening. Future work evaluating more subtle histological or functional effects may be prudent before such treatments are initiated. In particular, studies should validate that no neuronal loss occurs as a result of the procedure. While no cell loss was evident here, since we sonicated both hemispheres in each animal we were unable to compare cell counts in sonicated vs. non-sonicated structures. Advanced methods for detecting BBB disruption below what we could



detect using MRI contrast and trypan blue may also be warranted to ensure that the barrier was fully intact outside of the targeted tissue volumes. The safety of delivering any given pharmaceutical agent into the brain should also be assessed before clinical tests.

These results confirm prior experiments in small animals, in which a safe window has been repeatedly found where BBB disruption is possible without tissue damage evident in light microscopy (32,39,40). This safe window was clear in this work, despite uncertainties in estimating the in vivo pressure amplitudes due to the effects of the skull, which were not corrected for here. The estimated threshold for BBB disruption, (50% probability at 149 kPa) is lower than the 272 kPa expected value based on similar analysis from small animal studies (14). This disparity may reflect issues with our acoustic calibrations, differences in the sonication parameters compared to earlier studies, or differences in thresholds that may exist between small animals and primates. The fact that trypan blue extravasation was observed in white matter but Gd-DPTA extravasation was not suggests that the BBB disruption threshold was lower than our estimates, as clearly there was a level that we could not detect using MRI.

The BBB disruption varied substantially from location-to-location, even using the same exposure level. This was found both for single-target (see Fig. 2, for example) and volumetric sonications. This variability was probably due to uncertainties in our estimates for the in vivo acoustic pressure amplitude due to the skull. While skull-induced aberration is expected to be minor at 220 kHz (41), there are brain regions where it may be more significant because of the incident angles between the transducer elements and the skull. Beyond a critical angle of  $\sim 25^\circ$ , the entire incident longitudinal acoustic wave is reflected (42). At more oblique angles, energy can be transmitted into the brain via shear waves generated in the skull, with more attenuation, but less beam aberration (42). At central locations such as the thalamus and putamen, most transducer elements will have incident angles less than the critical angle, and at very superficial targets such as the visual and cingulate cortices, most elements will have highly oblique incident angles. We observed good BBB disruption at both extremes, even without aberration correction. In contrast, the disruption achieved in deep, lateral targets such as the LGN/hippocampus was generally patchy and weak. Such targets had a large dispersion of incident angles, resulting in longitudinal and shear mode transmission for different parts of the transducer, potentially leading to poor focusing.

In addition to uncertainties in estimating the in vivo exposure levels, local differences in vascularity and consequent microbubble concentration may have played a role in the observed variability. Such differences could explain why Gd-DPTA extravasation was evident only in gray matter, which is highly vascularized compared to white matter. Future efforts in treatment planning would need to account for both the transmission through the skull and the local tissue vascularity. More sensitive contrast imaging than what was utilized here will also be needed to detect BBB disruption in white matter.

More consistent results could also be achieved with effective guidance and monitoring to control the ultrasound exposure level in real-time. These results demonstrate that monitoring acoustic emission is a promising mechanism for such control. We found that transcranial acoustic monitoring was feasible with this device, and acoustic emissions correlated with both contrast enhancement (with increased harmonic emission) and vascular damage (with wideband acoustic emission). These findings confirm previous small animal studies from our laboratory (32). In our ongoing tests of this device, we now routinely use this acoustic feedback to guide the exposure levels, and we plan to implement automated control over the sonication system to ensure safe and effective BBB disruption. Detailed analysis of the acoustic emissions will be presented in a subsequent manuscript.

## Conclusion

We demonstrated that focal BBB disruption can be reliably and repeatedly produced in a clinically-relevant animal model using a TcMRgFUS system designed for patient treatments, and that this disruption can be achieved without significant tissue damage or functional deficits. BBB disruption was found to be substantially less in white matter, where Gd-DPTA delivery was not detected with MRI. Behavioral testing indicates that function remains normal, even after multiple repeated BBB disruption sessions. These results are supportive of performing initial clinical tests of this noninvasive method for targeted drug delivery in the brain, at least for life-threatening conditions such as brain tumor.

## Supplementary Material

Refer to Web version on PubMed Central for supplementary material.

## Acknowledgments

The authors wish to thank Yongzhi Zhang and Vladimir Berezovskii for histology, Ron Watkins and Ehud Schmidt for their help with our MRI coil, and Omer Brokeman and Eyal Zadicario for their technical assistance with these experiments.

### Grant Support

This work was supported by award number RC2NS069413 from the National Institute of Neurological Disorders And Stroke. The content is solely the responsibility of the authors and does not necessarily represent the official views of the National Institute of Neurological Disorders And Stroke or the National Institutes of Health. The focused ultrasound system was supplied by InSightec. Additional support was provided by a gift from Betty Brudnick.

## References

1. Abbott NJ, Romero IA. Transporting therapeutics across the blood-brain barrier. *Mol Med Today*. 1996; 2(3):106–113. PMID: 8796867. [PubMed: 8796867]
2. Misra A, Ganesh S, Shahiwala A, Shah SP. Drug delivery to the central nervous system: a review. *J Pharm Pharm Sci*. 2003; 6(2):252–273. PMID: 12935438. [PubMed: 12935438]
3. Kroll RA, Neuwelt EA. Outwitting the blood-brain barrier for therapeutic purposes: osmotic opening and other means. *Neurosurgery*. 1998; 42(5):1083–1099. [PubMed: 9588554]
4. Pardridge WM. Blood-brain barrier delivery. *Drug Discov Today*. 2007; 12(1–2):54–61. PMID: 17198973. [PubMed: 17198973]
5. Eichler AF, Chung E, Kodack DP, Loeffler JS, Fukumura D, Jain RK. The biology of brain metastases—translation to new therapies. *Nat Rev Clin Oncol*. 2011; 8(6):344–356. PMID: 21487419. [PubMed: 21487419]
6. Fukumura D, Jain RK. Tumor microenvironment abnormalities: causes, consequences, and strategies to normalize. *J Cell Biochem*. 2007; 101(4):937–949. PMID: 17171643. [PubMed: 17171643]
7. Lockman PR, Mittapalli RK, Taskar KS, Rudraraju V, Gril B, Bohn KA, et al. Heterogeneous blood-tumor barrier permeability determines drug efficacy in experimental brain metastases of breast cancer. *Clin Cancer Res*. 2010; 16(23):5664–5678. PMID: 20829328. [PubMed: 20829328]
8. Hynynen K, McDannold N, Vykhodtseva N, Jolesz FA. Noninvasive MR imaging-guided focal opening of the blood-brain barrier in rabbits. *Radiology*. 2001; 220(3):640–646. PMID: 11526261. [PubMed: 11526261]
9. Hynynen K, McDannold N, Sheikov NA, Jolesz FA, Vykhodtseva N. Local and reversible blood-brain barrier disruption by noninvasive focused ultrasound at frequencies suitable for trans-skull sonications. *Neuroimage*. 2005; 24(1):12–20. PMID: 15588592. [PubMed: 15588592]
10. Sheikov N, McDannold N, Sharma S, Hynynen K. Effect of Focused Ultrasound Applied With an Ultrasound Contrast Agent on the Tight Junctional Integrity of the Brain Microvascular

- Endothelium. *Ultrasound Med Biol.* 2008; 34(7):1093–1104. PMID: 18378064. [PubMed: 18378064]
11. Shang X, Wang P, Liu Y, Zhang Z, Xue Y. Mechanism of Low-Frequency Ultrasound in Opening Blood-Tumor Barrier by Tight Junction. *J Mol Neurosci.* 2010; 43(3):364–369. PMID: 20852968. [PubMed: 20852968]
  12. Sheikov N, McDannold N, Jolesz F, Zhang YZ, Tam K, Hynynen K. Brain arterioles show more active vesicular transport of blood-borne tracer molecules than capillaries and venules after focused ultrasound-evoked opening of the blood-brain barrier. *Ultrasound Med Biol.* 2006; 32(9): 1399–1409. PMID: 16965980. [PubMed: 16965980]
  13. McDannold N, Vykhodtseva N, Hynynen K. Effects of Acoustic Parameters and Ultrasound Contrast Agent Dose on Focused-Ultrasound Induced Blood-Brain Barrier Disruption. *Ultrasound Med Biol.* 2008; 34(6):930–937. PMID: 18294757. [PubMed: 18294757]
  14. McDannold N, Vykhodtseva N, Hynynen K. Blood-brain barrier disruption induced by focused ultrasound and circulating preformed microbubbles appears to be characterized by the mechanical index. *Ultrasound Med Biol.* 2008; 34(5):834–840. PMID: 18207311. [PubMed: 18207311]
  15. Choi JJ, Selert K, Gao Z, Samiotaki G, Baseri B, Konofagou EE. Noninvasive and localized blood-brain barrier disruption using focused ultrasound can be achieved at short pulse lengths and low pulse repetition frequencies. *J Cereb Blood Flow Metab.* 2010; 31(2):725–737. PMID: 20842160. [PubMed: 20842160]
  16. Chopra R, Vykhodtseva N, Hynynen K. Influence of exposure time and pressure amplitude on blood-brain-barrier opening using transcranial ultrasound exposures. *ACS Chem Neurosci.* 2010; 1(5):391–398. PMID: 20563295. [PubMed: 20563295]
  17. Yang FY, Lin GL, Horng SC, Chang TK, Wu SY, Wong TT, et al. Pulsed high-intensity focused ultrasound enhances the relative permeability of the blood-tumor barrier in a glioma-bearing rat model. *IEEE Trans Ultrason Ferroelectr Freq Control.* 2011; 58(5):964–970. PMID: 21622052. [PubMed: 21622052]
  18. Kinoshita M, McDannold N, Jolesz FA, Hynynen K. Noninvasive localized delivery of Herceptin to the mouse brain by MRI-guided focused ultrasound-induced blood-brain barrier disruption. *Proc Natl Acad Sci U S A.* 2006; 103(31):11719–11723. PMID: 16868082. [PubMed: 16868082]
  19. Treat LH, McDannold N, Zhang Y, Vykhodtseva N, Hynynen K. Targeted delivery of doxorubicin to the rat brain at therapeutic levels using MRI-guided focused ultrasound. *Int J Cancer.* 2007; 121(4):901–907. PMID: 17437269. [PubMed: 17437269]
  20. Mei J, Cheng Y, Song Y, Yang Y, Wang F, Liu Y, et al. Experimental study on targeted methotrexate delivery to the rabbit brain via magnetic resonance imaging-guided focused ultrasound. *J Ultrasound Med.* 2009; 28(7):871–880. PMID: 19546329. [PubMed: 19546329]
  21. Liu HL, Hua MY, Chen PY, Chu PC, Pan CH, Yang HW, et al. Blood-brain barrier disruption with focused ultrasound enhances delivery of chemotherapeutic drugs for glioblastoma treatment. *Radiology.* 2010; 255(2):415–425. PMID: 20413754. [PubMed: 20413754]
  22. Jordao JF, Ayala-Grosso CA, Markham K, Huang Y, Chopra R, McLaurin J, et al. Antibodies targeted to the brain with image-guided focused ultrasound reduces amyloid-beta plaque load in the TgCRND8 mouse model of Alzheimer's disease. *PLoS ONE.* 2010; 5(5):e10549. PMID: 20485502. [PubMed: 20485502]
  23. Minniti G, Amelio D, Amichetti M, Salvati M, Muni R, Bozzao A, et al. Patterns of failure and comparison of different target volume delineations in patients with glioblastoma treated with conformal radiotherapy plus concomitant and adjuvant temozolomide. *Radiother Oncol.* 2010; 97(3):377–381. PMID: 20855119. [PubMed: 20855119]
  24. Dobelbower MC, Burnett Iii OL, Nordal RA, Nabors LB, Markert JM, Hyatt MD, et al. Patterns of failure for glioblastoma multiforme following concurrent radiation and temozolomide. *J Med Imaging Radiat Oncol.* 2011; 55(1):77–81. PMID: 21382192. [PubMed: 21382192]
  25. Chamberlain MC. Radiographic patterns of relapse in glioblastoma. *J Neurooncol.* 2011; 101(2): 319–323. PMID: 21052776. [PubMed: 21052776]
  26. Hynynen K, Clement GT, McDannold N, Vykhodtseva N, King R, White PJ, et al. 500-element ultrasound phased array system for noninvasive focal surgery of the brain: A preliminary rabbit

- study with ex vivo human skulls. *Magn Reson Med*. 2004; 52(1):100–107. PMID: 15236372. [PubMed: 15236372]
27. Pernot M, Aubry JF, Tanter M, Boch AL, Marquet F, Kujas M, et al. In vivo transcranial brain surgery with an ultrasonic time reversal mirror. *J Neurosurgery*. 2007; 106:1061–1066.
  28. McDannold N, Clement GT, Black P, Jolesz F, Hynynen K. Transcranial magnetic resonance imaging-guided focused ultrasound surgery of brain tumors: initial findings in 3 patients. *Neurosurgery*. 2010; 66(2):323–332. PMID: 20087132. [PubMed: 20087132]
  29. Martin E, Jeanmonod D, Morel A, Zadicario E, Werner B. High-intensity focused ultrasound for noninvasive functional neurosurgery. *Ann Neurol*. 2009; 66(6):858–861. PMID: 20033983. [PubMed: 20033983]
  30. Clement GT, Hynynen K. A non-invasive method for focusing ultrasound through the human skull. *Phys Med Biol*. 2002; 47(8):1219–1236. PMID: 12030552. [PubMed: 12030552]
  31. Tung YS, Marquet F, Teichert T, Ferrera V, Konofagou EE. Feasibility of noninvasive cavitation-guided blood-brain barrier opening using focused ultrasound and microbubbles in nonhuman primates. *Appl Phys Lett*. 2011; 98(16):163704. PMID: 21580802. [PubMed: 21580802]
  32. McDannold N, Vykhodtseva N, Hynynen K. Targeted disruption of the blood-brain barrier with focused ultrasound: association with cavitation activity. *Phys Med Biol*. 2006; 51(4):793–807. PMID: 16467579. [PubMed: 16467579]
  33. Lele, PP. Effects of ultrasound on "solid" mammalian tissues and tumors in vivo. In: Repacholi, MH.; Grondolfo, M.; Rindi, A., editors. *Ultrasound: Medical Applications, Biological Effects and Hazard Potential*. New York: Plenum Pub. Corp.; 1987. p. 275-306.
  34. Livingstone MS, Srihasam K, Morocz IA. The benefit of symbols: monkeys show linear, human-like, accuracy when using symbols to represent scalar value. *Anim Cogn*. 2010; 13(5):711–719. PMID: 20443126. [PubMed: 20443126]
  35. Bakay L, Hueter TF, Ballantine HT, Sosa D. Ultrasonically produced changes in the blood-brain barrier. *Arch Neurol*. 1956; 76:457–467.
  36. McDannold N, Vykhodtseva N, Raymond S, Jolesz FA, Hynynen K. MRI-guided targeted blood-brain barrier disruption with focused ultrasound: Histological findings in rabbits. *Ultrasound Med Biol*. 2005; 31(11):1527–1537. PMID: 16286030. [PubMed: 16286030]
  37. slicer.org [Internet]. Available from: <http://www.slicer.org>
  38. Gering DT, Nabavi A, Kikinis R, Grimson WEL, Hata N, Everett P, et al. An integrated visualization system for surgical planning and guidance using image fusion and interventional imaging. *Int Conf Med Image Comput Comput Assist Interv*. 2012; 2(809):819.
  39. Hynynen K, McDannold N, Vykhodtseva N, Raymond S, Weissleder R, Jolesz FA, et al. Focal disruption of the blood–brain barrier due to 260-kHz ultrasound bursts: a method for molecular imaging and targeted drug delivery. *J Neurosurgery*. 2006; 105:445–454. PMID: 16961141.
  40. Tung YS, Vlachos F, Choi JJ, Deffieux T, Selert K, Konofagou EE. In vivo transcranial cavitation threshold detection during ultrasound-induced blood-brain barrier opening in mice. *Phys Med Biol*. 2010; 55(20):6141–6155. PMID: 20876972. [PubMed: 20876972]
  41. Yin X, Hynynen K. A numerical study of transcranial focused ultrasound beam propagation at low frequency. *Phys Med Biol*. 2005; 50(8):1821–1836. PMID: 15815098. [PubMed: 15815098]
  42. Clement GT, White PJ, Hynynen K. Enhanced ultrasound transmission through the human skull using shear mode conversion. *J Acoust Soc Am*. 2004; 115(3):1356–1364. PMID: 15058357. [PubMed: 15058357]

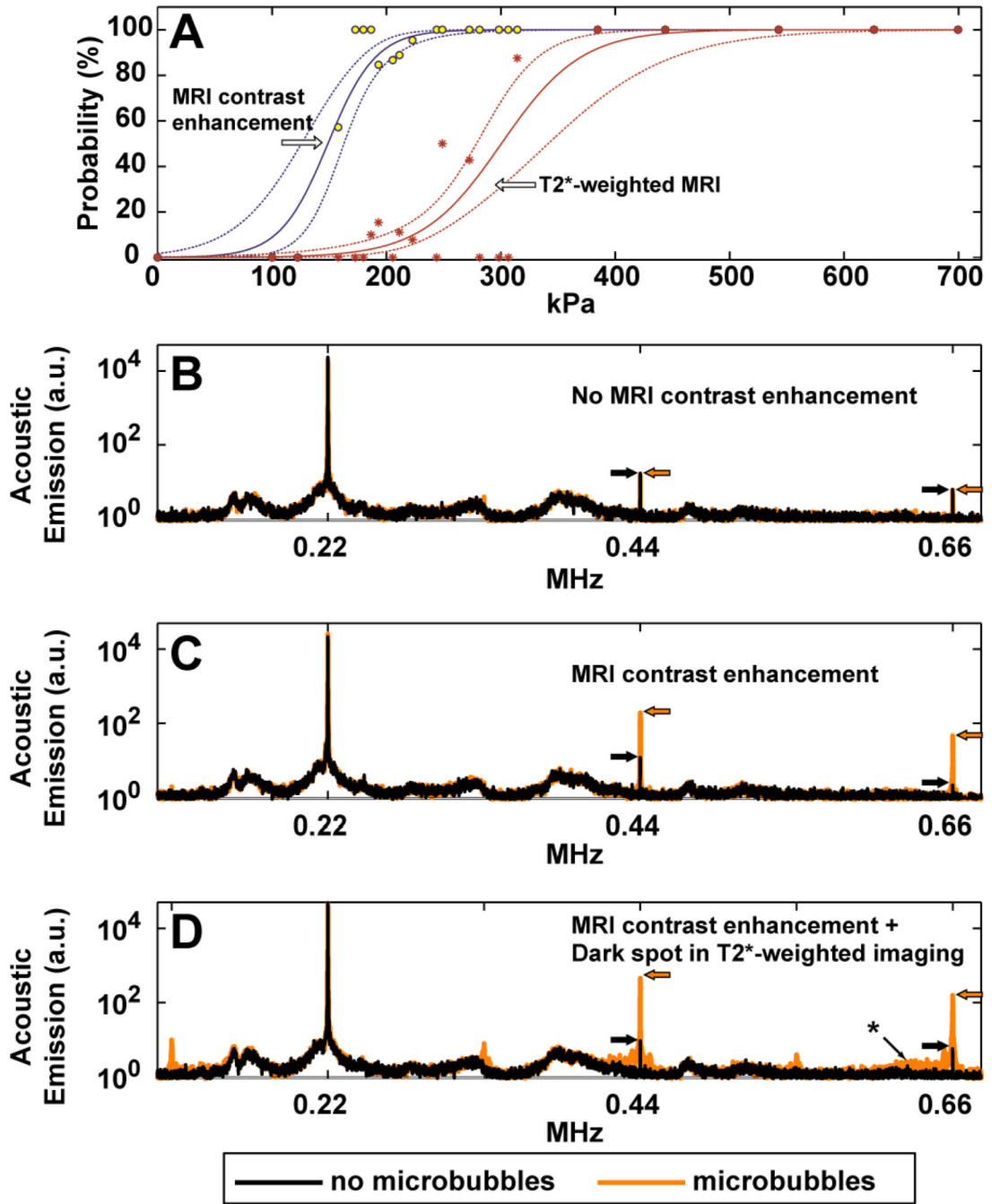


**Fig. 1.**  
**(A):** Estimation of the thresholds for BBB disruption and tissue damage in gray matter targets, as reflected in enhancement in contrast-enhanced T1-weighted imaging and hypointense spots in T2\*-weighted imaging, respectively. The individual data points show measured occurrences at the different exposure levels tested, which ranged from 100–700 kPa (acoustic power: 0.2–10 W). Solid lines show logistic regression of the data (dotted lines: 95% confidence intervals). A narrow window for BBB disruption without production of MRI-evident petechiae was found. **(B–D)** Acoustic emission measured during sonications at locations where MRI contrast enhancement was not observed **(B)**, was observed **(C)**, and

was accompanied by small dark spots in T2\*-weighted imaging, presumably from petechiae (**D**). Each location was sonicated twice, once without the microbubble USCA, and once with microbubbles. Without microbubbles, only small spectral peaks were observed at the second and third harmonics of the TcMRgFUS device. With microbubbles, sonicated locations where MRI contrast extravasation was observed showed a marked increase in this harmonic activity. The third harmonic signal magnitude was enhanced by 22 and 28 times on average with microbubbles for the examples shown in (**B**) and (**C**), respectively; no enhancement was observed after the sonication shown in (**A**). When dark spots were seen in T2\*-weighted imaging, additional emission was observed in the sensitive region of our detector (approximately 650 kHz, identified with an asterix), indicating that wideband emission – a signature of inertial cavitation – had occurred. Subharmonic and ultraharmonic emission (at 1/2, 3/2, and 5/2 of the TcMRgFUS frequency) was also observed in this example. The top and middle examples were in white matter and cortex targets, respectively, from one of the volumetric sonications shown in Fig. 4 (223 kPa). The bottom example was from a location in a volumetric sonication at 193 kPa in the visual cortex in monkey 5. The average of 20 spectra is shown in each case.

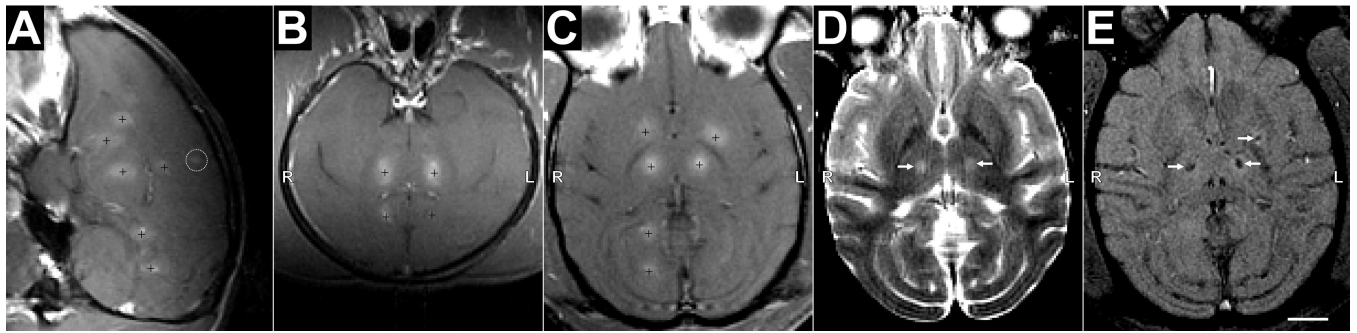


**Fig. 2.**

BBB disruption in monkey 3 after targeting individual points with focused ultrasound and microbubbles. The disruption was demonstrated by delivery of an MR contrast agent (Gd-DPTA) that does not normally extravasate in the brain. **(A)** Sagittal contrast-enhanced MRI showing BBB disruption at six targeted locations (indicated by “+”) in the right hemisphere. The enhancement was contained to the targeted region except for small enhancement in a sulcus (circled) that was close to the most superficial location, which overlapped the lateral ventricle. Even though the same exposure level (314 kPa) was used for each sonication in this hemisphere, the size and magnitude of the different disruptions varied. **(C)** Axial view. Locations on left hemisphere were targeted at 223–273 kPa. **(D)** Axial T2-weighted image showing edema formation at the two targets in the thalamus (arrows). **(E)** T2\*-weighted image showing hypointense spots at the thalamic targets as well as in a target in the putamen that was not evident in T2-weighted imaging. (scale bar: 1 cm

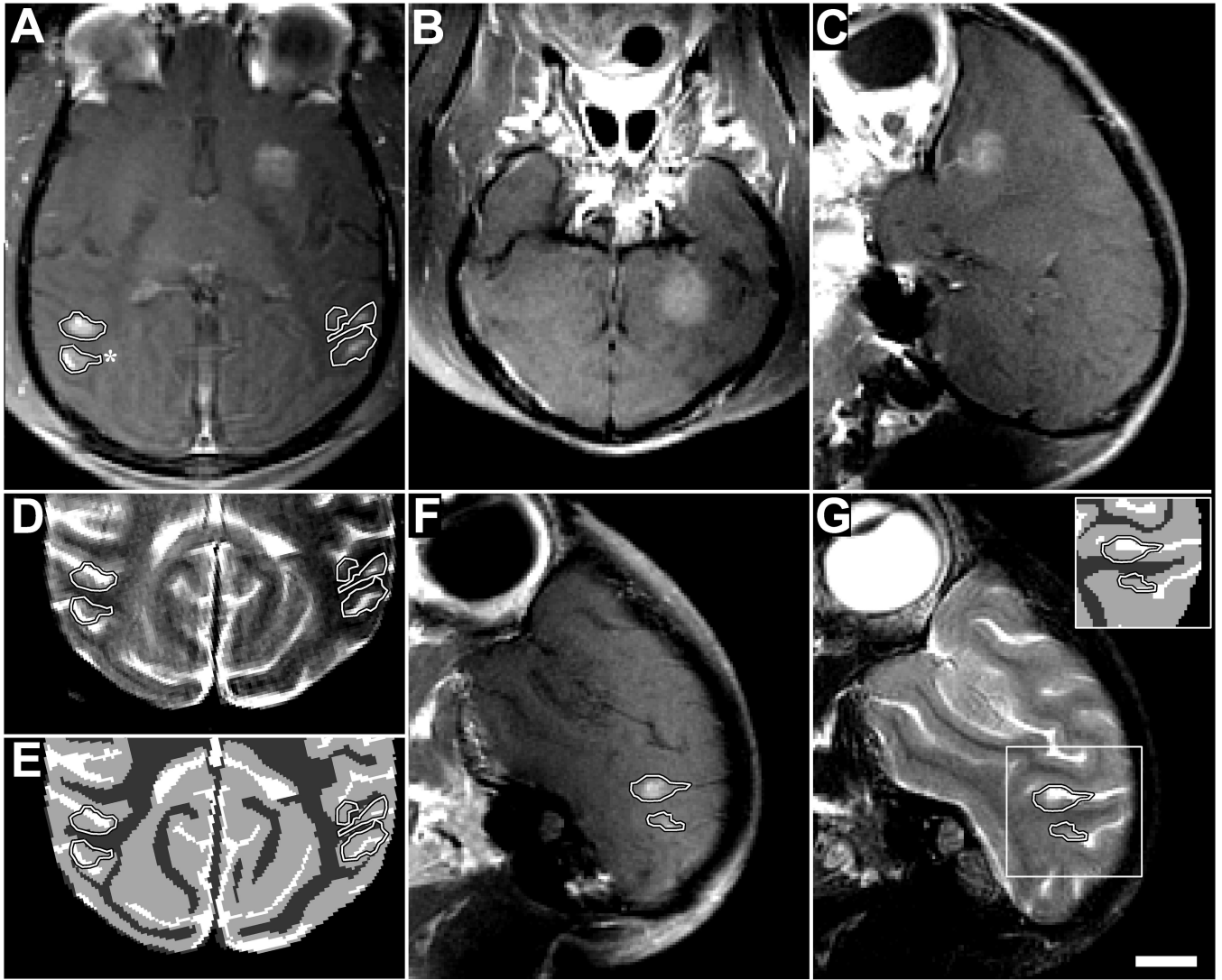


**Fig. 3.** Extravasation of Gd-DPTA after volumetric BBB disruption in the putamen and visual cortex in monkey 4 (223 kPa). Volumes were targeted by systematically steering to different locations in a 3×3 grid during the sonication. **(A)** Axial contrast-enhanced T1-weighted image showing homogeneous Gd-DPTA extravasation in the putamen, but inhomogeneous delivery in the visual cortex locations (outlined). **(B–C)** Coronal and sagittal views of volumetric Gd-DPTA extravasation in putamen. Note that no effects were observed at the beam path or at the skull base. **(D)** T2-weighted image with the enhancing areas observed in the visual cortex in **(A)** superimposed. **(E)** Segmentation of **(D)** into white matter (dark gray), gray matter (light gray), and cerebral spinal fluid (white). The areas of enhancement overlapped almost perfectly with the gray matter components of the sonication. **(F)** Sagittal view of enhancement in visual cortex. **(G)** Same view in T2-weighted image (inset: segmentation) showing enhancement only in gray matter. Histology findings from the enhancing area indicated by the asterix in **(A)** are shown in Fig. 5G–J (scale bar: 1 cm)



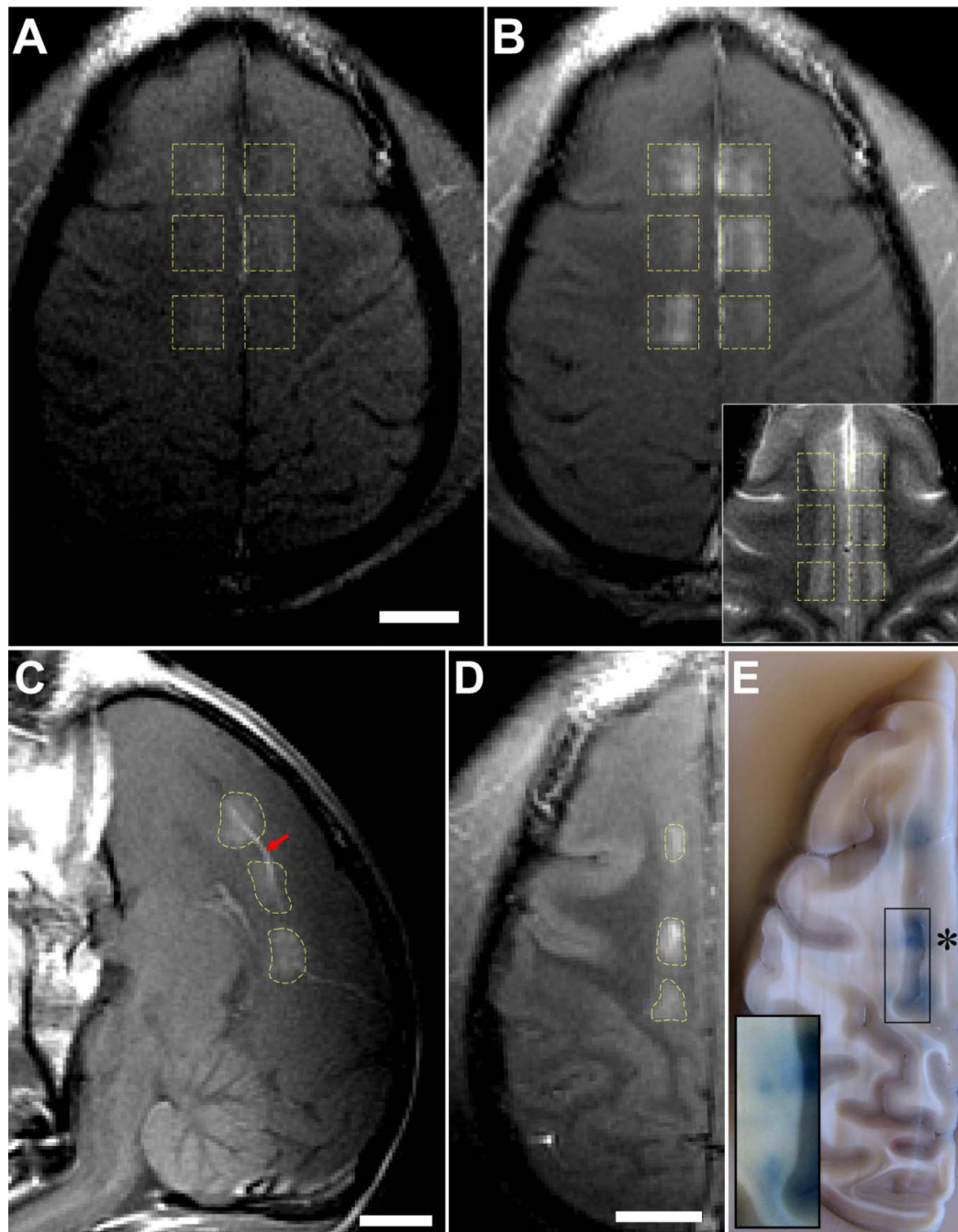


**Fig. 4.** Delivery of different tracers to the cingulate cortex in monkey 4. (**A–C**) Contrast-enhanced T1-weighted MRI after volumetric BBB disruption at six locations in the cingulate cortex (223 kPa). (**A**) Low-level enhancement observed with gadofosveset trisodium, an MR contrast agent that binds to albumin in the blood (MW of albumin: ~50 kDa); it was administered before sonication. (**B**) Enhancement after injection of Gd-DTPA (MW: 938 Da). The inset in (**B**) shows the same view in T2-weighted imaging. The enhancement patterns correspond to regions of cortical gray matter visible in T2-weighted imaging. (**C**) Sagittal view of Gd-DTPA enhancement, which included leakage of agent into a sulcus

(arrow). **(D–E)** Volumetric BBB disruption (223 kPa) at three targets centered on the boundary between the cingulate cortex and white matter; from the last session in monkey 4. **(D)** T1-weighted MRI showing Gd-DPTA extravasation in the cingulate cortex, but not in the white matter. **(E)** Photograph of formalin-fixed brain showing trypan blue extravasation into both the cingulate cortex and white matter. The white matter component of two of these targets is shown with increased image contrast in the inset to better visualize low-level trypan blue extravasation. Histology findings for the middle target (“\*”) are shown in Fig. 5A–F. No significant tissue damage was found as a result of these sonications. (scale bars: 1 cm

\$watermark-text

\$watermark-text

\$watermark-text

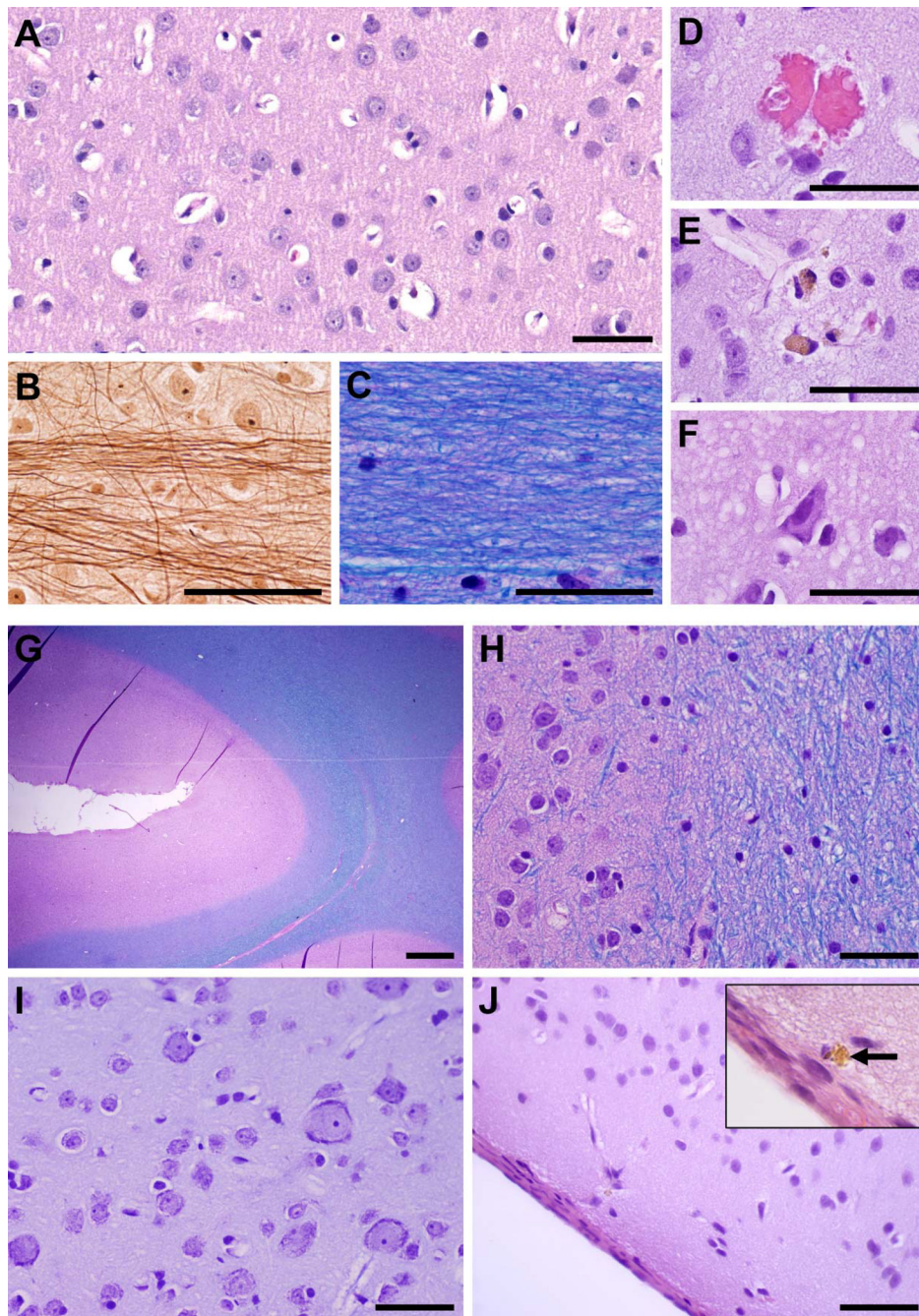


**Fig. 5.** Microphotographs showing representative histological findings after volumetric BBB disruption when abnormalities were not observed in T2\*-weighted imaging. **(A–F) Treatment site: middle cingulate cortex and adjacent white matter indicated by an asterisk in Fig. 4E.** This area was sonicated eight times over a period of several months. **(A)** Normal cingulate cortex; neurons and glia cells appear intact with no inflammatory cells present. **(B)** Bielschowsky's silver impregnation reveals normal axonal morphology within adjacent white matter at high magnification; **(C)** H&E-LFB shows preserved myelin. Evidence of the sonications was limited to a few injured capillaries **(D–F)**. **(D)** A small

group of extravasated red blood cells, presumably induced by sonication ~2h prior. Very few of such petechiae were observed in the whole section (four in this case). **(E)** Two macrophages containing hemosiderin, presumably remnants from petechiae induced during an earlier session months prior. **(F)** Dark, shrunken (ischemic) neurons and a slightly vacuolated neuropil found within a small (200–300  $\mu\text{m}$ ) affected area. **(G–J) Treatment site: visual cortex + subcortical white matter and sulcus, indicated by an asterix in Fig. 3.** This area was sonicated three times over several months. **(G–H)** Normal appearing cortex (pink) around a sulcus; intact white matter (blue) is seen at the right of the images. **(I)** No abnormalities were found in cortical gray under higher magnification. **(J)** The brain surface a few mm away from the targeted visual cortex appeared unaffected except for a few tiny hemosiderin deposits in the meninges or adjacent tissue, such as that shown in the inset. The cortical tissue just below the surface appeared normal. **(A, D–F, J: H&E; B: Bielschowsky's silver stain; C, G, H: H&E-LFB; I: Nissl; ; scale bars: G: 1 mm; others: 50  $\mu\text{m}$ )**

\$watermark-text

\$watermark-text

\$watermark-text

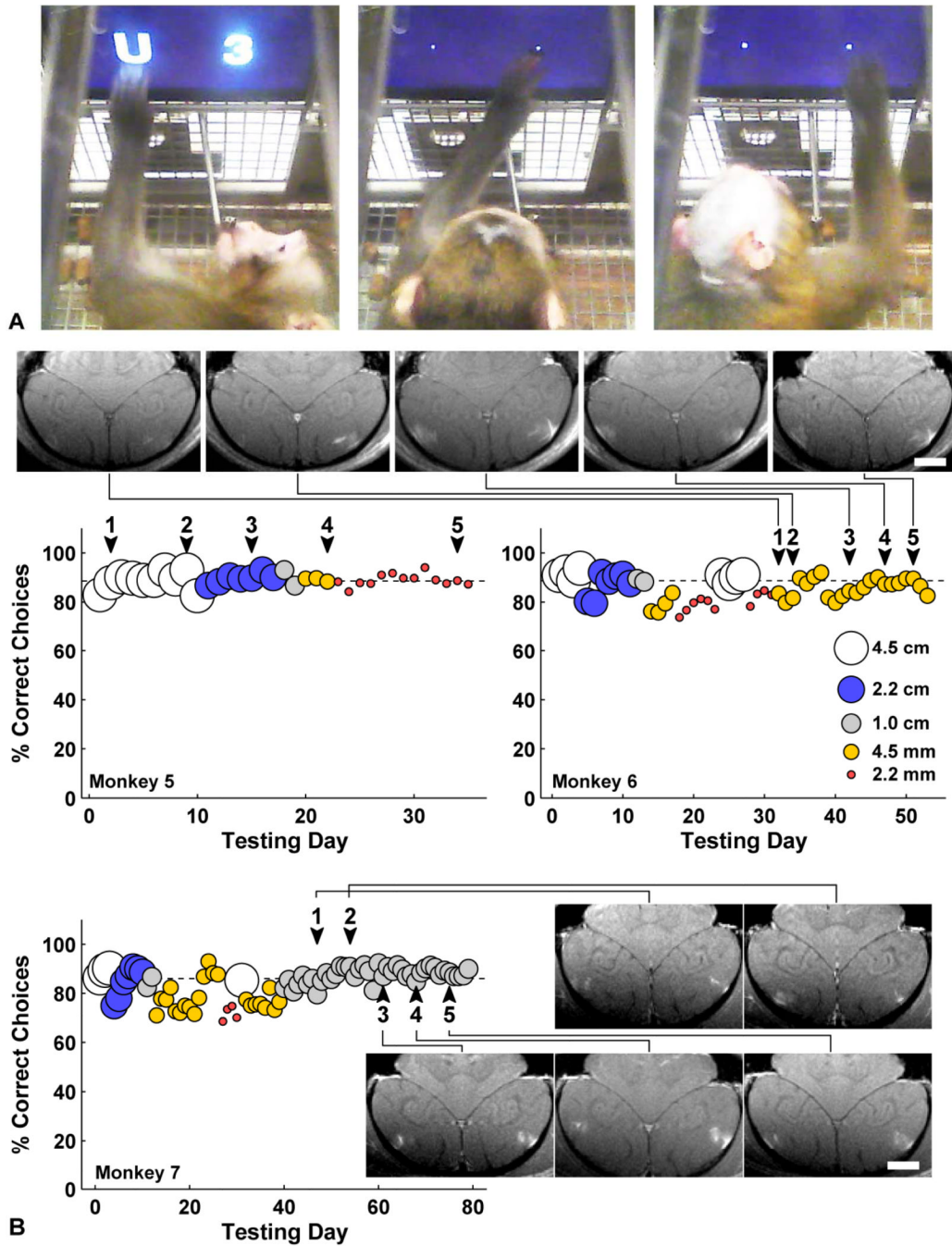


**Fig. 6.** (A) Two monkeys performing a visual discrimination test using in-cage touchscreen. They choose between two symbols representing different amounts of juice. Symbol size was reduced from 4.5 cm to 2 mm over time to test acuity. (Left) Monkey 5 choosing a 4.5 cm “U” (worth 15 drops) over “3” (3 drops); his mouth is on the juice tube. (Middle) Monkey 5 choosing a 2 mm “W” (12 drops) over “7” (7 drops). (Right) Monkey 6 choosing a 4 mm “A” (24 drops) over “K” (18 drops). The juice tube was 25 cm from the screen, so the 4.5 cm symbols subtended about 10° of visual angle, and 2 mm symbols subtended 0.5° visual angle. These video images were made 2 months after the last of five BBB disruptions in

monkey 5 and 48 h after the last of five BBB disruptions in monkey 6. **(B)** Daily performance of monkeys 5–7 before and after each of five sessions of BBB disruption to bilateral LGN and foveal visual cortex (arrowheads). The different symbol sizes are represented as indicated in the left graph. For monkey 5 the symbol size was gradually decreased between treatments, and for monkey 6 the second smallest symbol size was used throughout the treatment series. No decline in function or acuity was observed for any animal. Contrast-enhanced T1-weighted MRI showing bilateral volumetric BBB disruption in the gray matter components of the primary visual cortex over five successive sessions are shown for in monkey 6–7 (scale bars: 1 cm). In addition, volumes centered in the LGN were sonicated.

\$watermark-text

\$watermark-text

\$watermark-text